BBA - Bioenergetics 1860 (2019) 679–687

Contents lists available at ScienceDirect

BBA - Bioenergetics

journal homepage: www.elsevier.com/locate/bbabio

Interaction between γC87 and γR242 residues participates in energy coupling between catalysis and proton translocation in *Escherichia coli* ATP synthase☆

Yunxiang Li[a,b,*], Xinyou Ma[c], Joachim Weber[b,d]

[a] Department of Chemistry and Biochemistry, Texas Woman's University, Denton, TX 76204, USA
[b] Department of Chemistry and Biochemistry, Texas Tech University, Lubbock, TX 79409, USA
[c] Department of Chemistry, The University of Chicago, Chicago, IL 60637, USA
[d] The Center for Membrane Protein Research, Texas Tech University Health Sciences Center, Lubbock, TX 79430, USA

ARTICLE INFO

Keywords:
ATP synthase
Energy transmission
Molecular dynamics
Mutational study
Residue interaction

ABSTRACT

Functioning as a nanomotor, ATP synthase plays a vital role in the cellular energy metabolism. Interactions at the rotor and stator interface are critical to the energy transmission in ATP synthase. From mutational studies, we found that the γC87K mutation impairs energy coupling between proton translocation and nucleotide synthesis/hydrolysis. An additional glutamine mutation at γR242 (γR242Q) can restore efficient energy coupling to the γC87K mutant. Arrhenius plots and molecular dynamics simulations suggest that an extra hydrogen bond could form between the side chains of γC87K and β_{TP}E381 in the γC87K mutant, thus impeding the free rotation of the rotor complex. In the enzyme with γC87K/γR242Q double mutations, the polar moiety of γR242Q side chain can form a hydrogen bond with γC87K, so that the amine group in the side chain of γC87K will not hydrogen-bond with βE381. As a conclusion, the intra-subunit interaction between positions γC87 and γR242 modulates the energy transmission in ATP synthase. This study should provide more information of residue interactions at the rotor and stator interface in order to further elucidate the energetic mechanism of ATP synthase.

1. Introduction

F_1F_o ATP synthase plays a critical role in the cellular energy metabolism. A functional ATP synthase in *E. coli* requires the proper assembly of eight types of subunits in a stoichiometry of $ab_2c_{10}\alpha_3\beta_3\gamma\delta\varepsilon$ (See Supplementary Material Fig. S1A and B for the quaternary structure of the holoenzyme and the terminology used throughout this article) [1]. Its unique rotary mechanism couples two distinct functions: proton translocation and ATP synthesis/hydrolysis [2]. Considering that the binding locations of proton and nucleotide are approximately 100 Å apart [3], the central shaft γ subunit is essential to maintain the energy transmission in ATP synthase [4]. Protons flowing through two membrane half-channels in the a and c subunits push the rotor complex ($c_{10}\gamma\varepsilon$) to spin. The torque rotating the γ subunit within the $\alpha_3\beta_3$ cylinder alters the conformation of the nucleotide binding pockets in the β subunits to accomplish ATP synthesis [5]. Each of these three β subunits adopts a different conformation depending on the rotation angle of the γ subunit [6]. According to the nucleotide occupancy in the original crystal structure, those three β subunits are named as β_{TP} (AMP-PNP bound), β_{DP} (ADP bound) and β_E (empty) [7].

Functional energy conversion and transmission in ATP synthase require proper interactions between β and γ. Uncoupling can occur when the energy flow is disrupted. ATP cannot be synthesized when the proton gradient is dissipated otherwise; or *vice versa*, a proton gradient cannot be formed by ATP hydrolysis [8]. The importance of several conserved residues located at the β and γ interface was discovered in mutational studies. For instance, *E. coli* ATP synthase with βE381K, γS12A or γM23K mutations is incapable to use carbon source efficiently *in vivo* [4,9,10]. Residue γC87 is largely conserved, or occasionally replaced by alanine, but neither bulky nor charged amino are found in this position. γR242 in the C-terminus of the γ subunit is completely conserved (Supplementary Material Table S1). Previous studies have

Abbreviations: AMP-PNP, adenylyl-imidodiphosphate; CCCP, carbonyl cyanide *m*-chlorophenylhydrazone; MD, molecular dynamics

☆ *E. coli* numbering is used throughout this study.

* Corresponding author at: Ann Stuart Science Complex, P.O. Box 425859, Department of Chemistry and Biochemistry, Texas Woman's University, Denton, TX 76204-5859, USA.
E-mail address: yli7@twu.edu (Y. Li).

https://doi.org/10.1016/j.bbabio.2019.06.016
Received 10 April 2019; Received in revised form 19 June 2019; Accepted 22 June 2019
Available online 25 June 2019
0005-2728/ © 2019 Elsevier B.V. All rights reserved.

shown that *E. coli* ATP synthase with a γC87A mutation mirrors the WT behaviors in microbial growth yield, ATPase activity and ATP-driven proton pumping ability [4]. The cysteine at γC89 in spinach thylakoid ATP synthase (which is equivalent to γC87 in *E. coli*) is a target of H_2O_2 oxidation; the γC89A mutant can maintain high ATPase activity (85% of the WT) [11]. *E. coli* ATP synthase with γR242C mutation is WT-like, and it can restore the energy coupling caused by the γM23K mutation [12]. With the γR242E mutation in ATP synthase, no F_1 complex assembly on the membrane was found; a γM23K/γR242E double mutant cannot correct the energy uncoupling situation [9]. In the present study, we will investigate the interaction between γC87 and γR242 and its effect on modulation of energy transmission in ATP synthase.

2. Materials and methods

2.1. Strains

E. coli strain DH5α (New England BioLabs) was used for mutagenesis [13]. Strain DK8 (*glnV44*, *rfbC1*, *endA1*, *spoT1*, *hfrPO1*, *bglR*, *thi-1*, *relA1*, Δ(*atpB-atpC*) *ilv*::*Tn10*, Tetracycline resistant) was engineered by removing the *atp* (*unc*) operon from the chromosome of *E. coli* strain 1100 to yield a background without intrinsic ATP synthase [14,15].

2.2. Construction of plasmids

The pSN6 plasmid (pBR322 derivative, *atpB-atpC*, Ampicillin resistant) was used as the wild type (WT) throughout this study [16]. Oligonucleotides (Integrated DNA Technology, listed in Supplementary Material Table S2) for site-directed mutagenesis were applied in the polymerase chain reaction (PCR) by following the recommended protocol (Q5® High Fidelity DNA Polymerase, New England BioLabs). Presence of the desired mutation was verified by DNA sequencing, followed by transformation into strain DK8.

2.3. Growth yield assay

A single colony of DK8 strain harboring WT or mutant ATP synthase was inoculated in lysogeny broth (LB) medium with 100 μg/mL ampicillin and grown to late exponential phase. A further 1:500 inoculation was made into medium containing 8 mM succinate, allowing it to grow aerobically until saturation at 30 °C or 37 °C [17]. Growth yield was evaluated from turbidity of the liquid culture by measuring its absorbance at 590 nm. Each mutant was assayed at least in triplicate.

2.4. Inverted membrane vesicle preparations and protein concentration assay

Cells were pelleted at late exponential phase from aerobic growth at 30 °C. Resuspended cells were lysed by passage through a homogenizer. Membranes were then washed and pelleted as described [18]. For each strain expressing WT or mutant ATP synthase, at least two membrane vesicle preparations were made. Protein concentrations were determined by the Bradford method with bovine serum albumin as standard [19].

2.5. Western blot

The relative expression level of ATP synthase on membrane was determined by Western Blot with anti-β antibody (Agrisera, Vännas, Sweden) or anti-γ antibody (a kind gift from Drs. Toshiharu Suzuki and Masasuke Yoshida, Japan Science and Technology Agency, Tokyo) following standard protocols [20]. Band intensity was assessed by ImageJ software (National Institutes of Health). At least two biological replicate samples were quantified to minimize error.

2.6. Functional analysis of ATP synthase

ATPase activities were assayed in a cocktail buffer containing 50 mM Tris/H_2SO_4, 4 mM $MgSO_4$, 10 mM ATP and 1 μM carbonyl cyanide *m*-chlorophenylhydrazone (CCCP), pH 8.0, at 25 °C, 27 °C, 30 °C, 34 °C or 37 °C. To trigger the reaction, inverted membranes (10 μg/mL) were added into the cocktail buffer. To terminate the reaction, sodium dodecyl sulfate (SDS) was added to a final concentration of 5% (w/v). Inorganic phosphate released from the reaction was quantified as described [21]. Each membrane sample was assayed at least in duplicate. To test the membrane proton pumping ability, 50 μg/mL of inverted membrane vesicles were suspended under vigorous stirring in 2.0 mL proton pumping buffer containing 10 mM HEPES, 300 mM KCl, 5 mM $MgCl_2$, 1 μg/mL valinomycin and 1 μM acridine orange, pH 7.5, at 25 °C. Using an excitation wavelength of 460 nm, the acridine orange fluorescence intensity was measured at an emission wavelength of 530 nm. 1 mM ATP or 2 mM NADH was added to initiate proton pumping; 5 μM CCCP was added to dissipate the proton gradient [22]. Each sample was measured at least in duplicate.

2.7. Transition state thermodynamic parameters

The apparent enzyme activation energy for ATP hydrolysis by ATP synthase was obtained by measuring turnover number as a function of the temperature terms as given in the Arrhenius Eq. [23]. Turnover numbers were calculated by normalizing ATPase activities by the amount of membrane-bound ATP synthase determined by the Western Blot. Thermodynamic parameters can be resolved from the following equations:

$$\left[\frac{\partial \ln k_{cat}}{\partial(1/T)}\right]_p = -\frac{E_a}{R}$$

$$k_{cat} = Ae^{-\frac{E_a}{RT}}$$

$$E_a = \Delta H^{\ddagger} + RT$$

$$\Delta S^{\ddagger} = R\ln\left(\frac{AN_A h}{RT}\right) - R$$

$$\Delta G^{\ddagger} = \Delta H^{\ddagger} - T\Delta S^{\ddagger}$$

In these equations, R, A, N_A and h represent the ideal gas constant, Arrhenius constant, Avogadro's number and Planck constant respectively. k_{cat} is the turnover number; T, the absolute temperature, E_a, the Arrhenius activation energy, and G, H, S are Gibbs free energy, enthalpy and entropy terms [24].

2.8. Computational methods

Protein Data Bank (PDB) entry 3OAA (PDB ID: 3OAA) was adopted *in silico* as the parent protein model [25]. Chimera (University of California, San Francisco) software [26] was used to visualize the molecular structure of ATP synthase. Computational study of electrostatics in ATP synthase was conducted in Python 2.7 with AESOP (Analysis of Electrostatic Similarities of Proteins) module [27,28]. Directed mutagenesis scan function was programed with its default parameters to calculate the Gibbs free energy of subunit association (ΔG_a) in ATP synthase [29]. To introduce a mutation in the original structure, the rotamers function was used in Chimera, followed by energy minimizing to eliminate all clashes among residues using the default settings [30].

All-atom molecular dynamics (MD) simulations with explicit solvents were performed in GROMACS [31] with an AMBER99sb force field [32] for the WT, γC87K and γC87K/γR242Q mutants. Each protein was solvated in a cubic box with the simple point charge (SPC) water model and kept at least 10.0 Å from borders [33]. Na^+ and Cl^- ions were added into the system to neutralize charges in proteins at a

concentration of 150 mM. The long-range electrostatic interactions among ions and charges in proteins were solved with the Particle Mesh Eward (PME) method [34]. The solvated systems were optimized until the largest force component was < 10 kJ/(mol·nm) and equilibrated with the constrained protein conformations at 300 K and 1 atm over 200 ps. Unconstrained NPT MD simulations were numerically integrated for 5 ns at a time step of 2 fs, where trajectory information was saved using a 10 ps interval. The velocity rescaling thermostat method [35] and Parrinello-Rahman barostat method [36] were taken in equilibration steps and MD simulations.

3. Results

3.1. Mutation γC87K causes inefficient energy coupling in ATP synthase

Residue γC87 is highly conserved; occasionally, an alanine is found in this position (Supplementary Material Table S1). Alanine (small hydrophobic), aspartate, glutamate (acidic) and phenylalanine (bulky hydrophobic) substitutions were made in the mutational study. To evaluate the performance of the WT or mutant ATP synthase, growth yield in succinate medium, enzyme expression level, ATPase activity and ATP-driven proton pumping ability were measured. The γC87A/D/E mutants showed little adverse effect to the functions of ATP synthase, and they mirrored the WT in protein expression amount, ATPase activity and ATP-driven proton pumping ability. Strains carrying these mutations also maintained a substantial oxidative phosphorylation growth yield (> 80% compared to the WT) in 8 mM succinate medium. The γC87F mutant showed weaker ATP-driven proton pumping ability, as measured by acridine orange quenching, and lower growth yield (74% and 73% compared to the WT, respectively); however, it was still well capable to use non-fermentable carbon source efficiently.

Albeit γC87 is not absolutely essential, ATP synthase with γC87K mutation clearly presented a phenotype with poor utilization of succinate as the carbon source. Cells bearing such mutant enzyme hardly grew in succinate medium, resulting in a very low growth yield (< 20% at 30 °C, < 10% at 37 °C) compared to the WT. Western Blot assay found that the amounts of ATP synthase assembled on the cell membrane were similar in the WT and the γC87 mutants (Table 1). In addition, the *in vitro* ATPase activity assay and ATP-driven proton pumping assay illustrated that the γC87K mutant was able to hydrolyze ATP with 60% of the velocity as the WT, but it could barely convert the chemical energy released from ATP hydrolysis to establish a transmembrane proton gradient (< 10% ATP-driven proton pumping ability compared to the WT). The NADH-driven proton pumping assay clarified that the poor proton gradient observed with ATP was not because of passive leakage from damaged membrane vesicles. NADH-driven proton pumping by the γC87K mutant gave acridine orange quenching signal of 75% of WT; this slight reduction might be due to leakage through the uncoupled ATP synthase proton channel. All these observations indicated that the γC87K mutation impaired the energy coupling between ATP hydrolysis/synthesis and proton translocation across membrane in *E. coli* ATP synthase (Table 1). The γC87K mutant does not abolish all functions, but it is able to support a small amount of oxidative phosphorylation *in vivo*. This result provides evidence that there should not be any severe structural or assembly defects in the holoenzyme since it still can utilize the transmembrane proton gradient (in contrast to the free F_1 complex of ATP synthase, which is completely uncoupled).

3.2. Mutation γR242Q can suppress the energy uncoupling in the γC87K mutant

Residue γR242 is located in a conserved region in the C-terminus of γ subunit; it appears strictly conserved (Supplementary Material Table S1). From the crystal structure of *E. coli* ATP synthase (PDB ID: 3OAA) [25], the η-N atom of γR242 and the γ-S atom of γC87 are within 5 Å, so that an electrostatic repulsion might be caused by the γC87K mutation. A random mutation at the γR242 position was engineered by site-directed mutagenesis into the γC87K mutant. DK8 cells harboring ATP synthase with double mutations were screened on 20 mM succinate agar medium, resulting in colonies of different sizes. Plasmids were purified from the large colonies for DNA sequencing. This mutagenesis strategy successfully discovered a second site revertant: γR242Q (CAA). Compared to the γC87K mutant (17% at 30 °C, 8% at 37 °C of WT), cells with the double mutations showed better growth yield (85% at 30 °C, 90% at 37 °C) in succinate medium. Moreover, the ATP-driven proton pumping strength was restored to 52% compared to the WT (Table 2 and Fig. 1B).

Table 1
Energy coupling properties of γC87 mutants.

Strain	Growth yield	ATP synthase amount	ATPase activity	ATP-driven H^+ pumping	NADH-driven H^+ pumping
	%	%	unit/mg protein	%	%
WT	100	100	4.6 (0.8)	100	100
γC87A	95 (2)	90 (10)	3.9 (0.2)	88 (5)	90 (5)
γC87D	92 (3)	90 (10)	5.7 (0.3)	101 (3)	ND
γC87E	84 (3)	130 (20)	7.5 (0.4)	92 (4)	ND
γC87F	74 (4)	90 (10)	5.1 (0.4)	73 (5)	ND
γC87K	17 (2)	80 (10)	2.8 (0.5)	6 (3)	75 (6)
pUC18	< 1	0	< 0.01	< 1	99 (1)

DK8 strain expressing WT, mutant or no ATP synthase was allowed to grow in 8 mM succinate medium at 30 °C until saturation. Growth yield was quantified from the turbidity of cell culture by measuring absorbance at 590 nm. The membrane-bound ATP synthase amount was measured by Western Blot using anti-γ antibody. ATPase activities were determined by the amount of inorganic phosphate released at 37 °C; 1 unit is defined as 1 μmol inorganic phosphate released per minute. To evaluate proton pumping ability of ATP synthase, inverted cell membrane vesicles were suspended in proton pumping buffer. Either 1 mM ATP or 2 mM NADH was added to initiate proton pumping across membrane. Acridine orange fluorescence intensities were monitored at emission wavelength 530 nm with excitation wavelength at 460 nm. 5 μM CCCP was added to terminate the reaction and to establish 100% fluorescence intensity. All percentage values in this table are normalized against WT. Standard deviations are shown in parenthesis. DK8 with pUC18 plasmid serves as a negative control, harboring no *atp* operon. ND, not determined; since these mutants showed WT-like ATP-driven proton pumping ability, their membrane vesicles should maintain integrity.

3.3. γR242A/C/S are weak suppressors of γC87K

To further explore the function of γR242, alanine, cysteine, glutamate, leucine and serine replacements were engineered into the WT and the γC87K mutant. The γR242A/C/L/S mutants alone showed nearly WT-like growth yield, enzyme expression amount and enzymatic performance (Table 2 and Fig. 1A). In contrast, the γR242E mutant showed lowered growth yield, especially under higher temperature (66% at 30 °C, 30% at 37 °C). A previous study indicated that the γR242E mutation would interfere with ATP synthase assembly in cell membrane when *E. coli* cells were grown at 37 °C [9]. In the present study, the membranes were prepared from cells that grown at 30 °C, and ATP synthase was found assembled in the cell membranes by Western Blot and ATPase activity and proton pumping assay. Higher temperature appears to destabilize ATP synthase assembly in the γR242E mutant.

Regarding to the restoration of energy coupling, a double mutant with γC87K and γR242A, C or S mutations could grow well in succinate medium at 30 °C (~70% growth yield) but had worse performance at 37 °C (~30% growth yield only). γC87K/γR242E or γC87K/γR242L double mutants had low growth yield (~30% at 30 °C, < 10% at 37 °C), indicating that neither glutamate nor leucine in this position could

Table 2
Suppressor mutations at γR242 restore energy coupling in ATP synthase.

Strain	Growth yield		ATP synthase amount	ATPase activity	ATP-driven H^+ pumping	NADH-driven H^+ pumping
	30 °C %	37 °C %	%	unit/mg protein	%	%
WT	100	100	100	4.6 (0.8)	100	100
γC87K	17 (2)	8 (1)	80 (10)	2.8 (0.5)	6 (3)	75 (6)
γR242A	86 (4)	97 (3)	110 (10)	4.9 (0.5)	76 (5)	84 (3)
γR242C	95 (3)	98 (4)	110 (20)	2.4 (0.4)	87 (4)	95 (3)
γR242E	66 (4)	30 (3)	100 (10)	2.3 (0.4)	48 (4)	94 (3)
γR242L	81 (2)	85 (4)	100 (10)	2.4 (0.2)	56 (5)	85 (4)
γR242S	99 (2)	97 (4)	100 (10)	2.5 (0.3)	88 (4)	97 (2)
γC87K/γR242A	75 (4)	23 (4)	110 (10)	4.0 (0.6)	30 (3)	84 (3)
γC87K/γR242C	72 (3)	35 (3)	110 (20)	3.1 (0.4)	32 (4)	85 (5)
γC87K/γR242E	33 (4)	8 (2)	70 (10)	1.6 (0.2)	8 (2)	90 (3)
γC87K/γR242L	31 (3)	7 (2)	80 (10)	1.7 (0.2)	3 (2)	92 (3)
γC87K/γR242Q	85 (4)	90 (5)	110 (10)	4.5 (0.7)	52 (4)	80 (5)
γC87K/γR242S	73 (3)	22 (4)	110 (10)	4.0 (0.5)	45 (5)	72 (6)

Experimental conditions were as described in the legend of Table 1, except the growth yields were assayed at both 30 °C and 37 °C. All percentage values in this table are normalized against WT. Standard deviations are shown in parenthesis.

effectively correct the energy uncoupling issue. The proton pumping ability for each mutant showed the similar trends as the growth yield (Table 2 and Fig. 1B).

3.4. Mutations at γC87 and γR242 alter thermodynamic parameters of the transition state

In order to identify possible reasons for the inefficient energy coupling caused by the γC87K mutation, thermodynamic parameters were analyzed by Arrhenius plots (Supplementary Material Fig. S2A and B). The thermodynamic properties of γC87A/D/E/F mutations were very similar to those of WT; in sharp contrast, the γC87K enzyme showed an increased activation energy (WT + 19.4 kJ/mol). According to the transition state theory, this observation might indicate that extra interactions could occur between the γC87K and adjacent residues. Thus, more energy is required to overcome a higher activation energy barrier to reach the transition state in the γC87K mutant. If the raised activation energy could lead to the uncoupling phenotype of the γC87K mutation, a secondary suppressor mutation at γR242 should correct the altered thermodynamic parameters. As shown in Table 3, all the γR242A/C/Q/S mutants could somehow compensate the augmented activation energy in the γC87K mutant and restore the energy coupling capability. The γR242E mutant also showed a lowered activation energy, but it cannot well restore the efficient energy coupling because this glutamate replacement itself is found harmful to the function of ATP synthase. The γC87K/γR242L double mutant showed an even

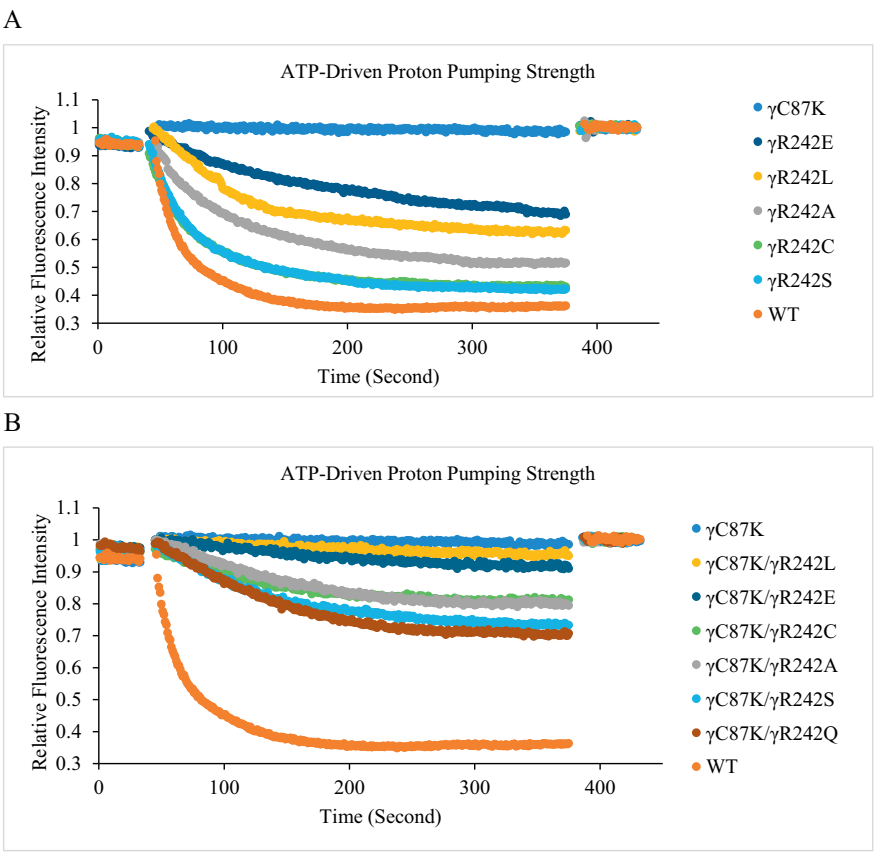

Fig. 1. Proton gradient formation ability of WT or mutant ATP synthase. The quenching of the fluorescence signal reflects the establishment of a proton gradient. ATP-driven proton pumping assay conditions were the same as described in the legend of Table 1. 1 mM ATP was added in the proton pumping buffer at Time = 40 s to initiate the proton translocation; 5 μM CCCP was added at Time = 385 s. (A) Proton pumping ability of γR242 mutants. (B) Proton pumping ability of γC87K with additional γR242 mutants.

Table 3
Transition state thermodynamic parameters of γC87 and γR242 mutants.

Strain	$\Delta H^{\ddagger}$ kJ/mol	$T\Delta S^{\ddagger}$ kJ/mol	$\Delta G^{\ddagger}$ kJ/mol
WT	33.6 (1.7)	−37.0 (1.7)	70.6 (0.0)
Strain	**$\Delta(\Delta H^{\ddagger})$ kJ/mol**	**$\Delta(T\Delta S^{\ddagger})$ kJ/mol**	**$\Delta(\Delta G^{\ddagger})$ kJ/mol**
γC87A	−2.9 (0.5)	−2.9 (0.5)	0.0 (0.0)
γC87D	−2.3 (1.0)	−1.3 (1.0)	−1.0 (0.0)
γC87E	−2.8 (0.3)	−1.1 (0.3)	−1.7 (0.0)
γC87F	+2.9 (0.6)	+3.6 (0.6)	−0.5 (0.0)
γC87K	+19.4 (2.3)	+17.0 (2.2)	−2.4 (0.1)
γC87K/γR242A	+1.8 (2.1)	+1.4 (2.0)	+0.4 (0.1)
γC87K/γR242C	+12.8 (1.1)	+11.4 (1.1)	+1.4 (0.0)
γC87K/γR242E	+12.2 (1.2)	+10.1 (1.2)	+2.1 (0.1)
γC87K/γR242L	+32.7 (0.4)	+30.1 (0.4)	+2.7 (0.0)
γC87K/γR242Q	+8.1 (0.9)	+7.8 (0.9)	+0.3 (0.0)
γC87K/γR242S	+1.4 (1.0)	+1.1 (1.0)	+0.3 (0.0)

ATPase activities of membrane-bound ATP synthase were measured at 25 °C, 27 °C, 30 °C, 34 °C and 37 °C. All terms were calculated for Arrhenius plots at 25 °C as described under Materials and Methods. ΔΔ values give the differences between mutant enzymes and the WT. Standard deviations are shown in parenthesis.

higher activation energy (WT + 32.7 kJ/mol) than the γC87K mutant and it failed to reform the functional energy transmission.

3.5. γC87 and γR242 residue may affect the subunit association

A mutagenesis analysis *in silico* was performed with the AESOP module to assess the influences of those γC87 and γR242 mutations. A single mutation was computationally engineered into ATP synthase once at a time. Through electrostatic stability evaluation among all the subunits ($\alpha_3\beta_3\gamma\varepsilon$ in PDB ID: 3OAA), a result returned as the Gibbs free energy change of subunit association (ΔG_a) for the parent structure (ΔG_a of WT = −21.5 kJ/mol) and each of the mutant (Fig. 2). The γC87K mutant presents a more negative ΔG_a value compared to its parent structure (WT – 12.3 kJ/mol). The γC87K mutation contributes to an overall electrostatic network and might make the ATP synthase too rigid to undergo conformational change smoothly. On the other hand, γR242 mutations weaken the overall electrostatic interaction to recover the flexibility in ATP synthase in the γC87K double mutants. This is especially true to the γR242E mutation, where the calculated ΔG_a is greater than zero (+10.1 kJ/mol), indicating that, based purely on electrostatic interactions, subunit association should not be favored. This result fits to the observations and it might explain the relative instability of the mutant enzyme [9]. This computational approach reinforced our hypothesis that the γC87K mutant would require higher energy to overcome the activation energy barrier and to achieve the transition state during nucleotide catalysis.

3.6. Molecular dynamics simulations reveal possible residue interactions

The MD simulation the trajectories of WT, γC87K and γC87K/γR242Q were visualized using Chimera. Fig. 3A, C and E show the residue conformation of the last frames from each MD simulation; distances among positions β_{TP}381, γC87, γ238 and γ242 are shown in Fig. 3B, D and F. Judged by enthalpy and protein backbone root-mean-square deviation (RMSD), equilibrium was reached after 2 ns. Hence, the unconstrained structures during the last 3 ns were used for residue interaction analysis. In the WT (Fig. 3A and B), the ensemble-averaged distance between γC87 (γ-S) and β_{TP}E381 (the nearer ε-O) is 6.1 ± 0.5 Å. The side chains of γR242 and γE238 form a hydrogen bond. In γC87K (Fig. 3C and D), the hydrogen bond between γR242 and γE238 remains, and an additional hydrogen bond is formed between γC87K and β_{TP}E381. The ensemble-averaged distance between γC87K (ζ-N) and β_{TP}E381 (the nearer ε-O) is 2.8 ± 0.1 Å. In the γC87K/γR242Q double mutant (Fig. 3E and F), hydrogen bonds between γC87K and β_{TP}E381 and between γR242 and γE238 are no longer present; a new hydrogen bond is formed between γC87K and γR242Q. In this conformation, the ensemble-averaged distance between γC87K (ζ-N) and β_{TP}E381 (the nearer ε-O) is 7.5 ± 0.4 Å. Compared with the inter-residue distances in the last 3 ns simulation (Fig. 3B, D and F), the distances in the WT show stronger fluctuations than those in the γC87K/γR242Q double mutant, and residues in the γC87K mutant are even less mobile than in the double mutant. This observation indicates that residues at this β/γ interface would be more rigid in γC87K than in the WT, and that the γC87K/γR242Q double mutations would allow a higher degree of flexibility to restore proper energy transmission.

4. Discussion

4.1. Energy transmission in ATP synthase

The long-term goal of this project is to illustrate the energy transmission mechanism in ATP synthase; our current target is the interface between the catalytic hexamer ($\alpha_3\beta_3$) and the γ subunit. Two areas

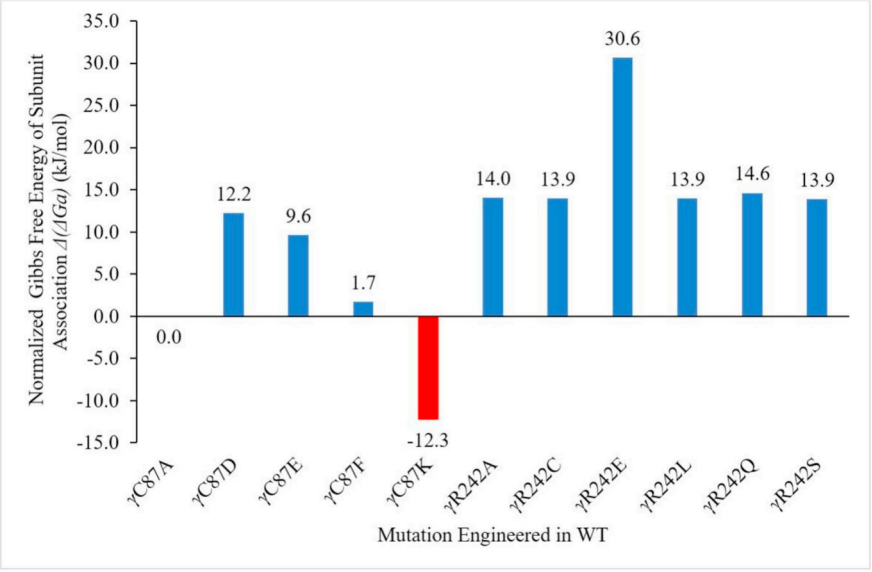

Fig. 2. Gibbs free energies of subunit association. Mutations were introduced *in silico* based on the structure of PDB ID: 3OAA. The overall electrostatic stability was calculated through the directed mutagenesis scan function in the AESOP module. This method suggests a thermal fluctuation with $kT \sim \pm 2.5$ kJ/mol [29]. The Gibbs free energy of subunit association for each mutant was normalized against the WT (−21.5 kJ/mol). A negative value of free energy of association in this figure indicates that the electrostatic interaction becomes stronger in the mutant ATP synthase, and it turns the enzyme into a more rigid complex compared to the parent structure.

have been identified as responsible for the energy transmission: one is located between the N- and C-terminal helices of γ and the upper β catch loop; the other one is located between γ "neck" cluster and the β^{380}DELSEED^{386} motif (the lower catch loop) [37]. Regarding the former area, previous studies have suggested that a network of hydrogen bonds and salt bridges is essential for communication between upper β catch loop and the coiled-coil helices of γ in *E. coli* ATP synthase, such as γS12 and βD372, γR268 and βD302/βD305 [10,38]. According to our recent study based on *Geobacillus stearothermophilus* ATP synthase, not individual amino acid side chain(s), but the overall

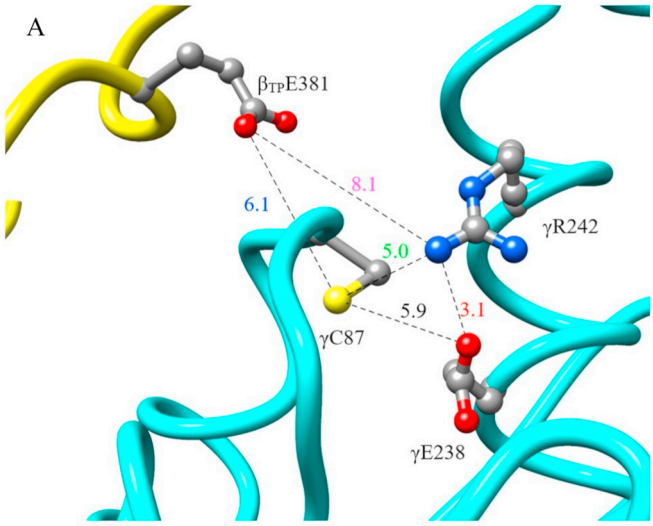

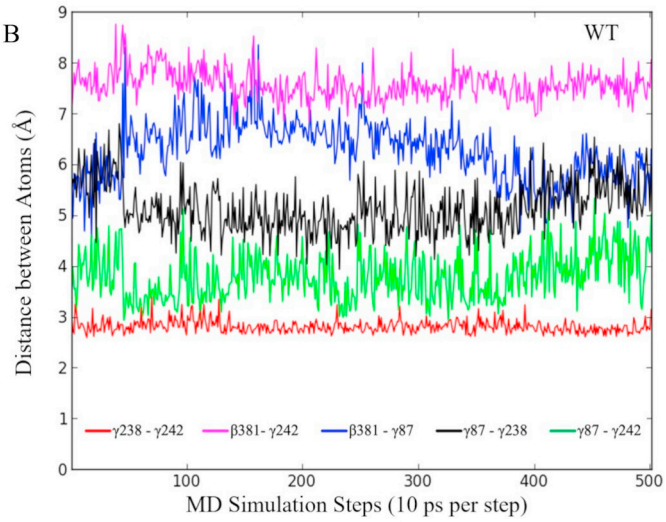

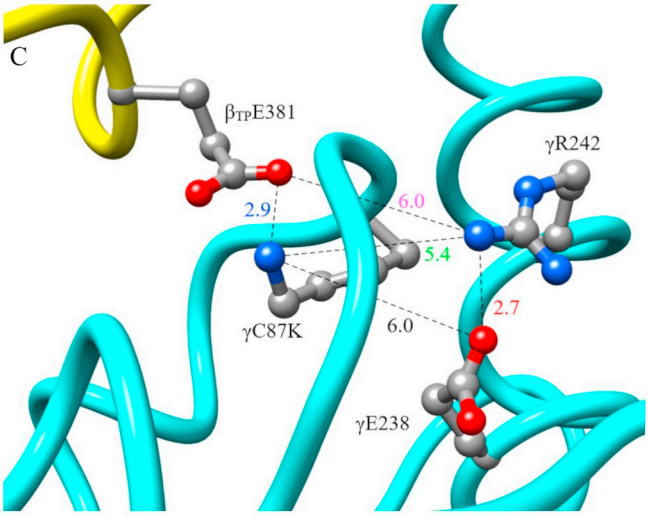

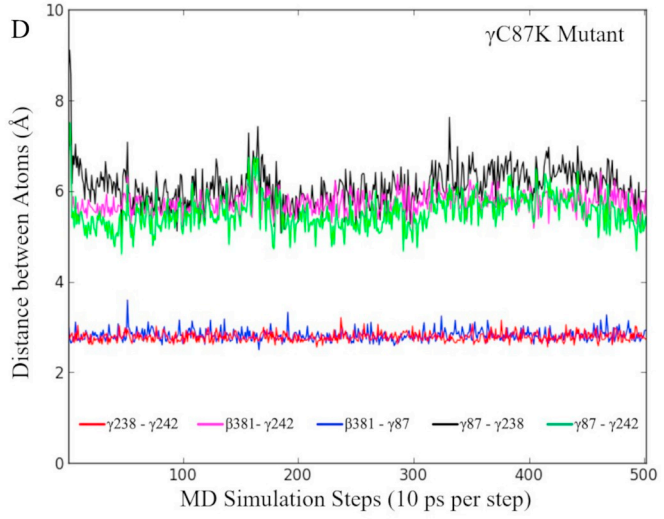

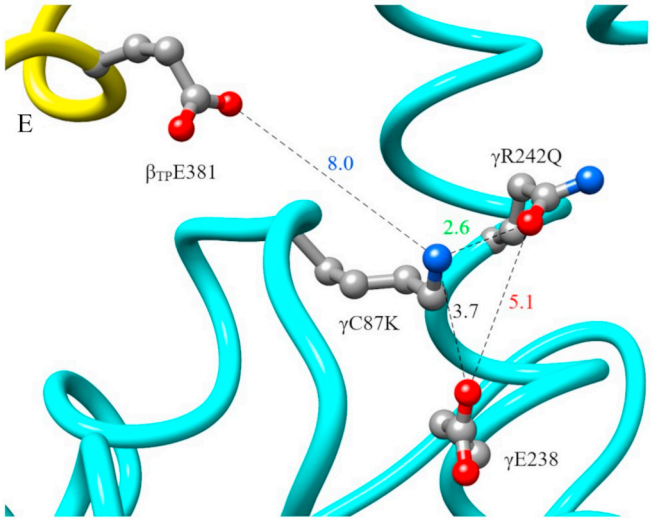

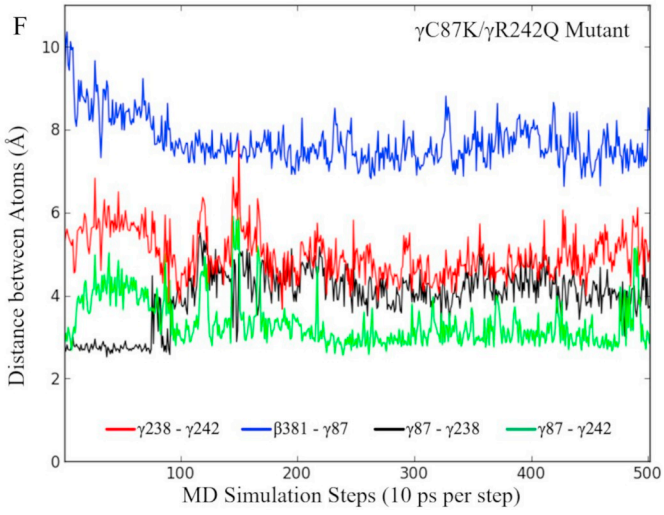

(caption on next page)

Fig. 3. Interactions of γC87 with the β_{TP}DELSEED loop. WT ATP synthase as well as γC87K and γC87K/γR242Q mutant structures were loaded into GROMACS for MD analysis. After 5 ns simulation, the last frame of each structure was illustrated by Chimera. In the Figs. A, C and E, β_{TP} and γ subunits are colored yellow and cyan respectively, and atoms are distinguished by CPK color mode (carbon element in gray, nitrogen in blue and oxygen in red). The distances between a pair of atoms are shown in Å. Figs. B, D and F show the distances between selected atoms *versus* the steps during MD simulations (10 ps per step). (A) WT ATP synthase. The distance between β_{TP}E381 (ε-O) and γC87 (γ-S) is 6.1 Å. (B) MD distances between atoms in WT. Red: γE238 (ε-O) and γR242 (η-N), Magenta: β_{TP}E381 (ε-O) and γR242 (η-N), Blue: β_{TP}E381 (ε-O) and γC87 (γ-S), Black: γC87 (γ-S) and γE238 (ε-O), Green: γC87 (γ-S) and γR242 (η-N). (C) γC87K ATP synthase. Due to electrostatic repulsion and spatial hindrance by γR242, the γC87K side chain folds toward β_{TP}E381. This increased β/γ interaction may restrict ATP synthase from normal rotation. The distance between β_{TP}E381 (ε-O) and γC87K (ζ-N) is 2.9 Å. (D) MD distances between atoms in the γC87K mutant. Red: γE238 (ε-O) and γR242 (η-N), Magenta: β_{TP}E381 (ε-O) and γR242 (η-N), Blue: β_{TP}E381 (ε-O) and γC87K (ζ-N), Black: γC87K (ζ-N) and γE238 (ε-O), Green: γC87K (ζ-N) and γR242 (η-N). (E) γC87K/γR242Q ATP synthase. Weakened charge repulsion from γR242Q allows the γC87K side chain to bond with γE238 and γR242Q itself. Moreover, the polar moiety of glutamine may further coordinate the γC87K side chain away from the β_{TP}DELSEED motif. The diminished interaction between γC87K and β_{TP}DELSEED rescues ATP synthase from inefficient energy coupling. In this model, the distance between β_{TP}E381 (ε-O) and γC87K (ζ-N) is 8.0 Å. (F) MD distances between atoms in the γC87K/γR242Q mutant. Red: γE238 (ε-O) and γR242Q (ε-O), Blue: β_{TP}E381 (ε-O) and γC87K (ζ-N), Black: γC87K (ζ-N) and γE238 (ε-O), Green: γC87K (ζ-N) and γR242Q (ε-O).

coiled-coil shape of the N- and C-terminal helices of γ is the key feature to maintain functional energy transmission [39]. In the latter area, the βDELSEED motif has been widely studied for its importance in the energy relay and torque generation [40–43].

4.2. Which part of ATP synthase would interact with γC87K?

Although the residue at γ87 is highly conserved among many species, it tolerates a mutation with small, bulky nonpolar or negatively charged side chain. The γC87K mutant fails to maintain the proper energy transmission and thus perturbs the coupling between proton translocation and ATP synthesis/hydrolysis. Both the transition state thermodynamic analysis and subunit association calculations strongly suggest that extra electrostatic interactions could form upon the replacement of cysteine by lysine. The positive charge on lysine could form a salt bridge or hydrogen-bond with adjacent residues. The βDELSEED motif is rich of negative charges. The βDELSEED sequence is greatly conserved among species (with only slight variations), but none of those five acidic residues is absolutely essential [20]. Many pieces of evidence support that the βDELSEED loop is involved in energy transmission through its conformational change upon nucleotide binding and release [43,44]. From the crystal structure of *E. coli* ATP synthase (PDB ID: 3OAA), γC87 (γ-S) is 6.1 Å away from β_{TP}E381 (ε-O); this distance would be even shorter upon the lysine replacement. Previous studies have reported that disulfide bonds form quickly between γC87 and βE381C as well as γC87 and βD380C under oxidizing conditions. As the covalent bond blocks rotation, ATP synthase abolishes both ATPase and proton pumping abilities [45,46]. The MD simulations reinforced our hypothesis. As shown in Fig. 3C, the bulky side chain of γR242 (η-N) might bond with γE238 (ε-O1) (2.7 Å), prohibiting the ionic interaction between γC87K (ζ-N) with γE238 (ε-O1) (6.0 Å). An additional salt bridge or hydrogen bond formed between γC87K (ζ-N) and β_{TP}DELSEED (2.9 Å to the ε-O of β_{TP}E381) could interfere with the normal rotation of ATP synthase.

4.3. How can a hydrogen bond between γC87K and β_{TP}DELSEED disturb the energy coupling?

ATP synthesis and release rely on the sequential conformational alternation of three β subunits, which is driven by the torque from the rotor complex ($c_{10}\gamma\varepsilon$) [47]. However, in *E. coli* ATP synthase, the rotation of γ and of the c-ring are not well matched. The γ subunit undergoes one revolution in three successive 120° steps, whereas the c-ring steps by ten 36° progressions [48]; consequently, protons pushing the c-ring produce a torque stored in the rotor complex due to its elasticity [49]. Coupled by this elastic torsion, the torque observed in the rotor complex changes little despite of its rotation angle [50]. Smooth torque transmission from the rotor to the catalytic hexamer enables high efficiency and optimal performance of ATP synthase [51].

When an extra hydrogen bond is formed between γC87K and β_{TP}E381, it drags the spin of the γ "neck" area. On the one hand, back slipping might occur when the torque generated from proton translocation is insufficient to overcome the elevated activation energy necessary for catalysis [52]. On the other hand, given the spin of γ "neck" motif is retarded while protons keep pushing the c-ring, the elastic energy built up within the rotor complex would be larger than in absence of the extra hydrogen bond [53]. When the elastic tension accumulated finally becomes large enough to break the hydrogen bond, the energy is released abruptly, with γ at more advanced rotational angle than usual. Such "jumpy" rotation of γ with a later release point of β-γ interactions would impact the energy transmission from the rotor complex to the catalytic hexamer and the subsequent conformational alternation of the β subunits. Neither back slipping nor "jumpy" spin of γ gives smooth and effective conformational change in the β subunits; hence, less ATP will be synthesized per time. In addition, considering the enzyme is not absolutely elastic, energy from proton gradient is consumed during unnecessary conformational change in ATP synthase, so that the energy coupling rate (ATP synthesis per proton) may become lower. This hypothesis can also explain the absence of an effect when γC87 is replaced by a neutral or acidic amino acid.

4.4. Efficient energy coupling in ATP synthase relies on a cluster consisting of γC87, γM23 and $\beta_{TP/DP}$E381

Previous studies have documented that the γM23K/R [22] and βE381K/R mutations [9,54] impair energy coupling between proton translocation and ATP synthesis/hydrolysis. Comparison with the results on the γC87K mutation from the present study shows similarities between these uncoupling mutations. First, they all have a side chain with a positive charge; second, they are spatially close to each other with potential interactions; third, they are all located at the βDELSEED/γ-neck interface which is critical to maintain efficient energy coupling (Fig. 4). With other types of mutation such as γM23D/E/L [4], γC87A/D/E/F (this study) and βE381A/D/Q [9], the functions of the enzyme are not affected. We propose that a high density of positive charge in this area prevents proper energy transmission in ATP synthase.

4.5. Intra-subunit communication between γC87 and γR242

The γR242C mutation can suppress inefficient energy coupling caused by the γC87K (this study) or the γM23K mutation [12]. A previous study on the γM23K/γR242C double mutant proposed that the cysteine residue in the γR242C mutation would remove the ionic bond between γR242 and βE381 and would form a repulsive ion pair between the thiolate and βE381 [55]. In that way, γR242C would be able to compensate the uncoupling effect of γM23K. Can we adopt the same idea to explain the observations with the γC87K mutation? First, it has to be pointed out that, although the γC87K and γM23K mutations share similarities in the thermodynamic patterns of the transition state, γC87K more likely interacts with β_{TP}E381 whereas the γM23K interacts with β_{DP}E381 [9]. Viewed from the original crystal structure (PDB ID: 3OAA) shown in Fig. 4, the distance between γR242 (η-N) and β_{TP}E381 (ε-O) or β_{DP}E381 (ε-O) residues is 8.2 Å and 14.8 Å respectively (β_EE381 is > 20 Å away and is inaccessible due to blockage by the helical portion of the γ subunit); thus,

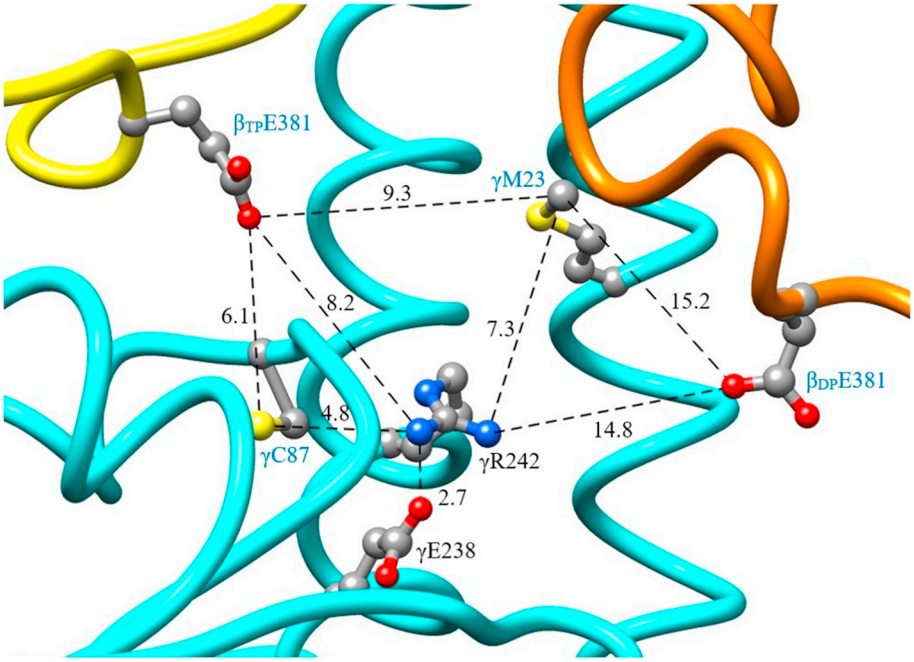

Fig. 4. Spatial relationship of residues located at the β and γ-neck interface. The figure is based on the crystal structure of *E. coli* ATP synthase (PDB ID: 3OAA). β_{TP}, β_{DP} and γ subunits are colored yellow, orange and cyan respectively. The CPK color mode is applied to distinguish different elements (carbon in gray, nitrogen in blue and oxygen in red). Distances among selected atom pairs are shown in Å. A residue labeled in blue shows that it has been reported (Refs. [9, 22, 54] or this study) to impair efficient energy coupling when replaced by lysine or arginine.

the diminished interaction between the γR242C mutant and βE381 may not significantly affect the enzyme rigidity during catalysis. Second, the pK_a value of a cysteine side chain is 8.5 (in water), and it requires a basic local environment to deprotonate the thiol into thiolate. Finally, except for γR242C, the charge repulsion hypothesis cannot explain other mutations such as γR242A/S/Q. Instead, most of the γR242 mutations are more likely to destabilize the interaction with γE238. The electrostatic attraction between γR242 and βE381 is not essential to ATP synthase, since many βE381 mutants [9,54] and γR242 mutants (this study) are WT-like.

How do the γR242 mutations interact with γC87K? If we accept the hypothesis that γC87K forms extra bonds with the βDELSEED motif resulting in energy transmission deficiency (Fig. 3C), in order to restore the functional energy flow, γR242 mutations should lead the γC87K away from the βDELSEED motif. At 30 °C, in the γR242A/C/S mutant, the less bulky side chain together with the removal of the positive charge seems to allow γC87K to bend back toward the interior of γ. The MD simulations (Fig. 3E) suggest that, although the side chain of γR242Q is not that small, its polar moiety can well hydrogen-bond to the lysine headgroup in γC87K (the distance between γC87K ζ-N to γR242Q ε-O is 2.8 Å). Furthermore, small or polar substitutions of γR242 could allow γC87K to form a salt bridge with γE238, thus stabilizing the lysine side chain (ζ-N) away from β_{TP}E381 (ε-O) (8.0 Å). At 37 °C, only γR242Q is able to correct the energy coupling issue satisfactorily. For side chains in position γR242 with weaker or no interactions with the lysine in position γ87 (such as γR242A/C/S), the increasing molecular freedom would give γC87K more flexibility to interact with the βDELSEED motif instead of γE238. γR242L can recover the energy coupling neither at 37 °C nor at 30 °C because its bulky and nonpolar side chain blocks γC87K bonding with γE238. The γR242E mutant alone already results in poor ATP-driven proton pumping ability and low growth yield; it is uncapable to correct the energy uncoupling issue in the ATP synthase with γC87K/γR242E double mutations either.

To summarize, γR242 has limited direct interaction with β_{TP}E381 but the residue in this position modulates the orientation of γC87K and affects its interaction with γE238. This discovery supports the notion that the residue communications at the β/γ interface are of crucial importance for energy transmission in ATP synthase.

Funding

This work was supported in part by the Robert A. Welch Foundation (m-0200) to the department of chemistry and biochemistry, Texas Woman's University. This work was also supported in part by NIH grant GM071462 (including ARRA Administrative Supplement) to JW.

Transparency document

The Transparency document associated with this article can be found, in online version.

Declaration of Competing Interest

The authors declare that there is no conflict of interest.

Acknowledgments

The authors would like to thank Drs. Mary E. Anderson, Richard D. Sheardy and Michael P. Latham for their many helpful discussions and kind assistance with instrumentation. The authors also acknowledge the Texas Advanced Computing Center (TACC, http://www.tacc.utexas.edu) at The University of Texas at Austin for providing the High-Performance Computing resources to this study.

Author contributions

Yunxiang Li: Conceptualization, Software, Validation, Formal analysis, Investigation, Project administration, Resources, Data curation, Writing - original draft, Writing - review & editing.

Xinyou Ma: Software, Formal analysis, Investigation, Resources, Writing - review & editing.

Joachim Weber: Conceptualization, Formal analysis, Resources, Writing - review & editing, Supervision, Funding acquisition.

Appendix A. Supplementary data

Supplementary data to this article can be found online at https://doi.org/10.1016/j.bbabio.2019.06.016.

References

[1] M. Sobti, C. Smits, A.S. Wong, R. Ishmukhametov, D. Stock, S. Sandin, A.G. Stewart, Cryo-EM structures of the autoinhibited *E. coli* ATP synthase in three rotational states, Elife. 5 (2016).

[2] J. Weber, Structural biology: toward the ATP synthase mechanism, Nat. Chem. Biol. 6 (2010) 794–795.

[3] D. Stock, A.G. Leslie, J.E. Walker, Molecular architecture of the rotary motor in ATP synthase, Science. 286 (1999) 1700–1705.

[4] K. Shin, R.K. Nakamoto, M. Maeda, M. Futai, F0F1-ATPase gamma subunit mutations perturb the coupling between catalysis and transport, J. Biol. Chem. 267 (1992) 20835–20839.

[5] H. Omote, N. Sambonmatsu, K. Saito, Y. Sambongi, A. Iwamoto-Kihara, T. Yanagida, Y. Wada, M. Futai, The gamma-subunit rotation and torque generation in F1-ATPase from wild-type or uncoupled mutant *Escherichia coli*, Proc. Natl. Acad. Sci. U. S. A. 96 (1999) 7780–7784.

[6] A.C. Hausrath, R.A. Capaldi, B.W. Matthews, The conformation of the epsilon- and gamma-subunits within the *Escherichia coli* F(1) ATPase, J. Biol. Chem. 276 (2001) 47227–47232.

[7] J. Weber, A.E. Senior, ATP synthesis driven by proton transport in F1F0-ATP synthase, FEBS Lett. 545 (2003) 61–70.

[8] T.L. Caviston, C.J. Ketchum, P.L. Sorgen, R.K. Nakamoto, B.D. Cain, Identification of an uncoupling mutation affecting the b subunit of F1F0 ATP synthase in *Escherichia coli*, FEBS Lett. 429 (1998) 201–206.

[9] C.J. Ketchum, M.K. Al-Shawi, R.K. Nakamoto, Intergenic suppression of the gammaM23K uncoupling mutation in F0F1 ATP synthase by betaGlu-381 substitutions: the role of the beta380DELSEED386 segment in energy coupling, Biochem. J. 330 (Pt 2) (1998) 707–712.

[10] D.S. Lowry, W.D. Frasch, Interactions between βD372 and γ subunit N-terminus residues γK9 and γS12 are important to catalytic activity catalyzed by *Escherichia coli* F1Fo-ATP synthase, Biochemistry. 44 (2005) 7275–7281.

[11] F. Buchert, Y. Schober, A. Rompp, M.L. Richter, C. Forreiter, Reactive oxygen species affect ATP hydrolysis by targeting a highly conserved amino acid cluster in the thylakoid ATP synthase gamma subunit, Biochim. Biophys. Acta 1817 (2012) 2038–2048.

[12] R.K. Nakamoto, M. Maeda, M. Futai, The gamma subunit of the *Escherichia coli* ATP synthase. Mutations in the carboxyl-terminal region restore energy coupling to the amino-terminal mutant gamma Met-23– > Lys, J. Biol. Chem. 268 (1993) 867–872.

[13] B.P. Anton, E.A. Raleigh, Complete genome sequence of NEB 5-alpha, a derivative of *Escherichia coli* K-12 DH5alpha, Genome Announc. 4 (2016).

[14] D.J. Klionsky, W.S. Brusilow, R.D. Simoni, In vivo evidence for the role of the epsilon subunit as an inhibitor of the proton-translocating ATPase of *Escherichia coli*, J. Bacteriol. 160 (1984) 1055–1060.

[15] B.J. Bachmann, Pedigrees of some mutant strains of *Escherichia coli* K-12, Bacteriol. Rev. 36 (1972) 525–557.

[16] H.Z. Mao, C.G. Abraham, A.M. Krishnakumar, J. Weber, A functionally important hydrogen-bonding network at the betaDP/alphaDP interface of ATP synthase, J. Biol. Chem. 283 (2008) 24781–24788.

[17] J. Weber, C. Bowman, S. Wilke-Mounts, A.E. Senior, Alpha-aspartate 261 is a key residue in noncatalytic sites of *Escherichia coli* F1-ATPase, J. Biol. Chem. 270 (1995) 21045–21049.

[18] C.S. Gajadeera, J. Weber, *Escherichia coli* F1Fo-ATP synthase with a b/delta fusion protein allows analysis of the function of the individual b subunits, J. Biol. Chem. 288 (2013) 26441–26447.

[19] M.M. Bradford, A rapid and sensitive method for the quantitation of microgram quantities of protein utilizing the principle of protein-dye binding, Anal. Biochem. 72 (1976) 248–254.

[20] N. Mnatsakanyan, S.K. Kemboi, J. Salas, J. Weber, The beta subunit loop that couples catalysis and rotation in ATP synthase has a critical length, J. Biol. Chem. 286 (2011) 29788–29796.

[21] H.H. Taussky, E. Shorr, A simplified method for estimating urinary inorganic phosphate during aluminum gel therapy for phosphatic calculi, J. Urol. 69 (1953) 454–455.

[22] C.J. Ketchum, R.K. Nakamoto, A mutation in the *Escherichia coli* F0F1-ATP synthase rotor, gammaE208K, perturbs conformational coupling between transport and catalysis, J. Biol. Chem. 273 (1998) 22292–22297.

[23] M.K. Al-Shawi, C.J. Ketchum, R.K. Nakamoto, Energy coupling, turnover, and stability of the F0F1 ATP synthase are dependent on the energy of interaction between gamma and beta subunits, J. Biol. Chem. 272 (1997) 2300–2306.

[24] M.K. Al-Shawi, A.E. Senior, Complete kinetic and thermodynamic characterization of the unisite catalytic pathway of *Escherichia coli* F1-ATPase. Comparison with mitochondrial F1-ATPase and application to the study of mutant enzymes, J. Biol. Chem. 263 (1988) 19640–19648.

[25] G. Cingolani, T.M. Duncan, Structure of the ATP synthase catalytic complex F(1) from *Escherichia coli* in an autoinhibited conformation, Nat. Struct. Mol. Biol. 18 (2011) 701–707.

[26] E.F. Pettersen, T.D. Goddard, C.C. Huang, G.S. Couch, D.M. Greenblatt, E.C. Meng, T.E. Ferrin, UCSF chimera - a visualization system for exploratory research and analysis, J. Comput. Chem. 25 (2004) 1605–1612.

[27] C.A. Kieslich, R.D. Gorham, D. Morikis, Is the rigid-body assumption reasonable? Insights into the effects of dynamics on the electrostatic analysis of barnase-barstar, J. Non-Cryst. Solids 357 (2011) 707–716.

[28] R.D. Gorham, C.A. Kieslich, A. Nichols, N.U. Sausman, M. Foronda, D. Morikis, An evaluation of Poisson-Boltzmann electrostatic free energy calculations through comparison with experimental mutagenesis data, Biopolymers. 95 (2011) 746–754.

[29] R.E.S. Harrison, R.R. Mohan, R.D. Gorham Jr., C.A. Kieslich, D. Morikis, AESOP: a python library for investigating electrostatics in protein interactions, Biophys. J. 112 (2017) 1761–1766.

[30] M.V. Shapovalov, R.L. Dunbrack, A smoothed backbone-dependent Rotamer library for proteins derived from adaptive kernel density estimates and regressions, Structure. 19 (2011) 844–858.

[31] S. Páll, M.J. Abraham, C. Kutzner, B. Hess, E. Lindahl, Tackling exascale software challenges in molecular dynamics simulations with GROMACS in: Solving software challenges for Exascale. EASC 2014. Lecture notes in computer science, Solving Softw. Challenges Exascale, 2015.

[32] V. Hornak, R. Abel, A. Okur, B. Strockbine, A. Roitberg, C. Simmerling, Comparison of multiple amber force fields and development of improved protein backbone parameters, Proteins Struct. Funct. Genet. 65 (2006) 712–725.

[33] D. Van Der Spoel, P.J. Van Maaren, H.J.C. Berendsen, A systematic study of water models for molecular simulation: derivation of water models optimized for use with a reaction field, J. Chem. Phys. 108 (1998) 10220–10230.

[34] T. Darden, D. York, L. Pedersen, Particle mesh Ewald: an N·log(N) method for Ewald sums in large systems, J. Chem. Phys. 98 (1993) 10089–10092.

[35] G. Bussi, D. Donadio, M. Parrinello, Canonical sampling through velocity rescaling, J. Chem. Phys. 126 (2007) 014101.

[36] R. Martoňák, A. Laio, M. Parrinello, Predicting crystal structures: the Parrinello-Rahman method revisited, Phys. Rev. Lett. 90 (2003) 075503.

[37] J. Pu, M. Karplus, How subunit coupling produces the gamma-subunit rotary motion in F1-ATPase, Proc. Natl. Acad. Sci. U. S. A. 105 (2008) 1192–1197.

[38] M.D. Greene, W.D. Frasch, Interactions among γR268, γQ269, and the β subunit catch loop of *Escherichia coli* F1-ATPase are important for catalytic activity, J. Biol. Chem. 278 (2003) 51594–51598.

[39] N. Mnatsakanyan, Y. Li, J. Weber, Identification of two segments of the subunit of ATP synthase responsible for the different affinities of the catalytic nucleotide-binding sites, J. Biol. Chem. 294 (2019, 1152-1160).

[40] K.Y. Hara, H. Noji, D. Bald, R. Yasuda, K. Kinosita Jr., M. Yoshida, The role of the DELSEED motif of the beta subunit in rotation of F1-ATPase, J. Biol. Chem. 275 (2000) 14260–14263.

[41] M. Tanigawara, K.V. Tabata, Y. Ito, J. Ito, R. Watanabe, H. Ueno, M. Ikeguchi, H. Noji, Role of the DELSEED loop in torque transmission of F1-ATPase, Biophys. J. 103 (2012) 970–978.

[42] T. La, G.D. Clark-Walker, X. Wang, S. Wilkens, X.J. Chen, Mutations on the N-terminal edge of the DELSEED loop in either the alpha or beta subunit of the mitochondrial F1-ATPase enhance ATP hydrolysis in the absence of the central gamma rotor, Eukaryot. Cell 12 (2013) 1451–1461.

[43] R. Watanabe, K. Koyasu, H. You, M. Tanigawara, H. Noji, Torque transmission mechanism via DELSEED loop of F1-ATPase, Biophys. J. 108 (2015) 1144–1152.

[44] J.R. Gledhill, M.G. Montgomery, A.G. Leslie, J.E. Walker, How the regulatory protein, IF(1), inhibits F(1)-ATPase from bovine mitochondria, Proc. Natl. Acad. Sci. U. S. A. 104 (2007) 15671–15676.

[45] Y. Zhou, T.M. Duncan, R.L. Cross, Subunit rotation in *Escherichia coli* FoF1-ATP synthase during oxidative phosphorylation, Proc. Natl. Acad. Sci. U. S. A. 94 (1997) 10583–10587.

[46] Z. Feng, R. Aggeler, M.A. Haughton, R.A. Capaldi, Conformational changes in the *Escherichia coli* ATP synthase (ECF1F0) monitored by nucleotide-dependent differences in the reactivity of Cys-87 of the gamma subunit in the mutant betaGlu-381 – > Ala, J. Biol. Chem. 271 (1996) 17986–17989.

[47] J. Czub, H. Grubmuller, Torsional elasticity and energetics of F1-ATPase, Proc. Natl. Acad. Sci. U. S. A. 108 (2011) 7408–7413.

[48] H. Sielaff, H. Rennekamp, A. Wachter, H. Xie, F. Hilbers, K. Feldbauer, S.D. Dunn, S. Engelbrecht, W. Junge, Domain compliance and elastic power transmission in rotary FOF1-ATPase, Proc. Natl. Acad. Sci. 105 (2008) 17760–17765.

[49] J.L. Martin, R. Ishmukhametov, D. Spetzler, T. Hornung, W.D. Frasch, Elastic coupling power stroke mechanism of the F1-ATPase molecular motor, Proc. Natl. Acad. Sci. U. S. A. 115 (2018) 5750–5755.

[50] O. Panke, D.A. Cherepanov, K. Gumbiowski, S. Engelbrecht, W. Junge, Viscoelastic dynamics of actin filaments coupled to rotary F-ATPase: angular torque profile of the enzyme, Biophys. J. 81 (2001) 1220–1233.

[51] W. Junge, H. Sielaff, S. Engelbrecht, Torque generation and elastic power transmission in the rotary F(O)F(1)-ATPase, Nature. 459 (2009) 364–370.

[52] M. Sekiya, R.K. Nakamoto, M.K. Al-Shawi, M. Nakanishi-Matsui, M. Futai, Temperature dependence of single molecule rotation of the *Escherichia coli* ATP synthase F1 sector reveals the importance of gamma-beta subunit interactions in the catalytic dwell, J. Biol. Chem. 284 (2009) 22401–22410.

[53] D.A. Cherepanov, A.Y. Mulkidjanian, W. Junge, Transient accumulation of elastic energy in proton translocating ATP synthase, FEBS Lett. 449 (1999) 1–6.

[54] S. Azim, Z. Ahmad, Glu residues of betaDELSEED-motif are essential for peptide binding in *Escherichia coli* ATP synthase, Int. J. Biol. Macromol. 116 (2018) 977–982.

[55] M.K. Al-Shawi, R.K. Nakamoto, Mechanism of energy coupling in the FOF1-ATP synthase: the uncoupling mutation, gammaM23K, disrupts the use of binding energy to drive catalysis, Biochemistry. 36 (1997) 12954–12960.